Implication of radioactive nuclear reaction ^{11}C(α, p)^{14}N in Supernova ν-process nucleosynthesis*

Xingqun Yao (姚星群)[1†] Yudong Luo (罗煜东)[2‡] Toshitaka Kajino[1,3,4§] Seiya Hayakawa[4,5] Hidetoshi Yamaguchi[4]
Xiaodong Tang (唐晓东)[6] Bingshui Gao (高丙水)[6] Fulong Liu (刘伏龙)[7,8]

[1]School of Physics, Peng Huanwu Collaborative Center for Research and Education, and International Research Center for Big-Bang Cosmology and Element Genesis, Beihang University, Beijing 100191, China
[2]School of Physics, Peking University, and Kavli Institute for Astronomy and Astrophysics, Peking University, Beijing 100871, China
[3]National Astronomical Observatory of Japan, 2-21-1 Osawa, Mitaka, Tokyo 181-8588, Japan
[4]Center for Nuclear Study, The University of Tokyo, RIKEN campus, 2-1 Hirosawa, Wako, Saitama 351-0198, Japan
[5]NanoTerasu Center, National Institutes for Quantum Science and Technology, 468-1 Aramaki Aza-Aoba, Aoba-ku, Sendai, Miyagi 980-8572, Japan
[6]Institute of Modern Physics, Chinese Academy of Sciences, Lanzhou 730000, China
[7]China Institute of Atomic Energy, Beijing 102413, China
[8]Center for Nuclear Study (CNS), the University of Tokyo, RIKEN Campus, 2-1 Hirosawa, Wako, Saitama 351-0198, Japan

Abstract: The origin of boron in the solar system has not yet been clearly understood. We studied the light mass nuclear reactions and neutrino-induced reactions that play important roles in the nucleosynthesis of A=11 nuclei in the core-collapse supernova (CCSN). We found that the production of A=11 nuclei, particularly ^{11}C, is sensitive to the radioactive nuclear reaction ^{11}C$(\alpha, p)^{14}$N among many others. We calculated the upper and lower limits of the ^{11}C$(\alpha, p)^{14}$N rate by taking account of the low energy resonances above the threshold, which have not been included in the previous SN nucleosynthesis calculations. These resonance contributions significantly change the ^{11}C abundance, which decays to ^{11}B with a half-life of 20.34 m, and affects the resultant isotopic abundance ratio of ^{11}B/^{10}B at $M_r = 3.78 - 4.4 M_\odot$ from which the presolar X grains could form. The ^{11}B/^{10}B isotopic ratio measured in X grains can help to understand the origin of solar system boron and constrain still unknown neutrino mass hierarchy if the observational and theoretical uncertainties associated with these abundances are reduced. We emphasize that the further precise experiment of measuring the ^{11}C$(\alpha, p)^{14}$N reaction cross sections at the astrophysically interesting energies of Gamow window 0.23−1.24 MeV, which corresponds to the effective temperature $T = 0.2 - 1$ GK, could clarify CCSN contribution to the solar ^{11}B/^{10}B ratio.

Keywords: Core-collapse supernova, explosive nucleosynthesis, reaction rates, nuclear physics

DOI: 10.1088/1674-1137/add680 **CSTR:** 32044.14.ChinesePhysicsC.49084003

I. INTRODUCTION

The boron in the solar system possibly originates from two primary astrophysical sources: spallation reactions in galactic cosmic ray (GCR), *i.e.* the collisions of high-energy charged particles with abundant p, ^{4}He and CNO nuclei in the interstellar medium (ISM) [1−3], and neutrino-induced nucleosynthesis (ν-process) in CCSN, *i.e.*, the neutrino spallation reactions in CCSN such as $\nu + {}^{12}\mathrm{C} \rightarrow {}^{11}\mathrm{B} + n$, ^{11}C+$p$ (^{11}C is a short-lived radioactive nucleus) [4] and the reaction chain such as ^{4}He(ν_e, p) ^{3}H$(\alpha, \gamma)^7$Li$(\alpha, \gamma)^{11}$B [5, 6]. Therefore, the two stable boron isotopes ^{10,11}B can serve as suitable probes for studying the explosion mechanism and ν-process nucleosynthesis in the CCSN.

Type X silicon carbide grains (hereafter *X grains*) are discovered in primitive meteorites [7, 8], and the isotopic ratios in X grains are valuable signatures that they are formed in the ejecta from CCSN [9]. The ^{11}B/^{10}B isotopic ratios measured in those X grains is 4.68 ± 0.31 [10, 11], which exceeds the solar values $(^{11}\mathrm{B}/^{10}\mathrm{B})_\odot \approx 4.04$ [12] by 2σ (here we take $\sigma \approx 0.31$). Standard GCR spallation

Received 8 March 2025; Accepted 8 May 2025; Published online 9 May 2025

* X. Yao was under the support of CSC scholarship from the Ministry of Education of China during his stay at the National Astronomical Observatory of Japan (NAOJ). T. Kajino was partly supported by the National Key R&D Program of China (2022YFA1602401) and the National Natural Science Foundation of China (12335009, 12435010). The work of H. Yamaguchi was supported by JSPS KAKENHI (19K03883, 23H01181, 23K25877) from the Ministry of Education, Culture, Sports, Science and Technology (MEXT) of Japan. Xingqun Yao and Yudong Luo contributed equally to this work

† E-mail: sternyao@buaa.edu.cn
‡ E-mail: yudong.luo@pku.edu.cn
§ E-mail: kajino@buaa.edu.cn

models predict $(^{11}B/^{10}B)_{GCR} \approx 2.5$ [2], which is significantly lower than both observed ratios in the solar system and X grains. This discrepancy may indicate that the ν-process in the CCSNe could be a dominant contribution to the solar system ^{11}B [3, 13, 14]. It has recently been indicated theoretically that the isotopic ratios such as $^{11}B/^{10}B$, $^{138}La/^{139}La$, etc. could help to constrain the still unknown neutrino mass hierarchy [15]. However, the existence of laboratory contamination in meteoritic observation prevents a clear conclusion on the origin of X grains [10, 11]. If the uncertainties from X grain data and theoretical calculation of the isotopic abundances can be reduced, these intrinsic $^{11}B/^{10}B$ ratios obtained from X grains will provide a unique window to study the explosive nucleosynthesis and the explosion mechanism of CCSN, and the chemical evolution in the early solar system.

Boron is a fragile nucleus and can be easily destroyed by the reactions such as $^{10}B(p,\alpha)^7Be$ and $^{11}B(p,2\alpha)^4He$ during the hydrogen burning process in the stellar evolution [12, 16, 17]. This also applies to the explosive SN ν-process nucleosynthesis because once ^{10}Be ($\tau_{1/2}$ = 1.51 My), ^{10}B, ^{10}C ($\tau_{1/2}$ = 19.3 s), ^{11}Be ($\tau_{1/2}$ = 13.8 s), ^{11}B and ^{11}C ($\tau_{1/2}$ = 20.34 m) are produced by the ν-spallation reactions, some fractions are quickly consumed by secondary destruction reactions. During the supernova explosion, the ^{6,7}Li, ^{7}Be, ^{10,11}B are produced and/or destroyed efficiently by the time when the temperature drops to $T \sim 0.2$ GK. After this time, the temperature and density quickly decrease as the materials are ejected into interstellar space (see Figure 1 of [5]). Therefore, even the fragile nuclei Li and B do not suffer further nuclear destruction processes and survive in the cooled materials until the SiC X grains condense and form after a few years but within 30 years [9, 18, 19]. Fujiya et al. discovered the ^{6,7}Li and ^{10,11}B isotopes in SiC X grains [11]. Our previous paper [15] discussed supernova nucleosynthesis of ^{6,7}Li and ^{10,11}B and their observability in X grains. The sensitivity of ^{11}B and ^{11}C abundances to the related nuclear reactions has not been studied in the literature and needs further careful investigation, particularly at the astrophysically important temperature range $T \leq 1$ GK for SN nucleosynthesis. We studied all the 43 nuclear reactions related to ^{11}B and ^{11}C from the JINA reaclib [20], and our analysis revealed that the secondary nuclear reaction, $^{11}C(\alpha,p)^{14}N$, is one of the most efficient reactions that destroys the ^{11}C and affect the final ^{11}B abundance. The present precision of experimental measurement of the reaction cross section is quite limited, especially at astrophysical low energies 0.23−1.24 MeV of Gamow window corresponding to $T = 0.2-1$ GK. The sensitivity of ^{11}C abundance to the $^{11}C(\alpha,p)^{14}N$ reaction rate requires further detailed study both experimentally and theoretically.

In the present work, we calculated the $^{11}C(\alpha,p)^{14}N$ S-factor by including the contributions from low energy resonances, which were ignored in the previous studies, and estimated the corresponding reaction rate and its associated uncertainty. Additionally, we investigated the impact of the new rate on the CCSN nucleosynthesis of the A=10 and A=11 nuclear systems to infer the sensitivity of ^{11}B production to the reaction rate. In Section II, we present the calculation of $^{11}C(\alpha,p)^{14}N$ S-factor and nuclear reaction rate in detail. In Section III, we discuss the effects of our new $^{11}C(\alpha,p)^{14}N$ rate on ^{11}B and ^{11}C production as well as their sensitivities in CCSN nucleosynthesis. The conclusion is given in Section IV.

II. $^{11}C(\alpha,p)^{14}N$ REACTION RATE

We perform a systematic study for all the 43 nuclear reactions related to the ^{11}B and ^{11}C production by enlarging and reducing each reaction rate by two orders of magnitude. These large multiplication factors are artificially introduced to identify the most sensitive nuclear reaction clearly, since the non-linear effect due to multiple reactions makes it challenging to find the net change of the A=11 nuclear abundances by only a single reaction if a much smaller factor is adopted. The reaction cross section for $^{11}C(\alpha,p)^{14}N$ has not been measured at astrophysical low energies $E \leq 0.6$ MeV as shown in Fig. 1. If we take account of five resonances at much lower energies,

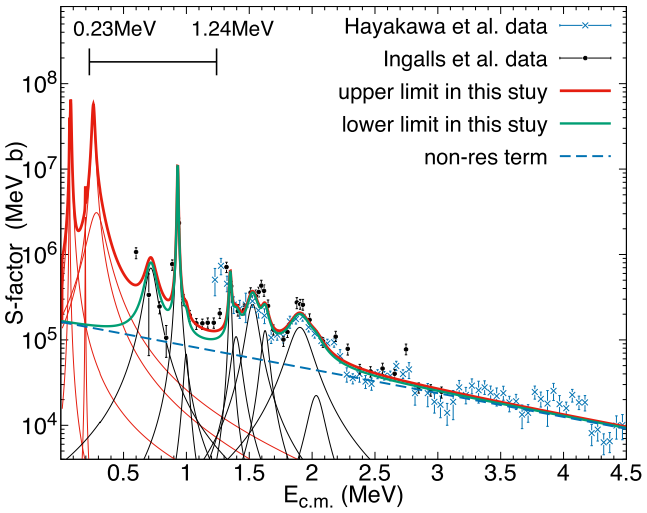

Fig. 1. (color online) Astrophysical S-factor of the reaction $^{11}C(\alpha,p)^{14}N$. Experimental data are from Ingalls data (black dots) and Hayakawa data (blue cross). The thick red line is the best fitting S-factor of the upper limit ($\theta_\alpha^2 = 1$ for i = 1−5). The thick dashed blue line is the non-resonant contribution. The thick green line is the lower limit of S-factor, which does not include the contribution of the lowest five resonances ($\theta_\alpha^2 = 0$). Thin red curves are the contributions from the lowest five resonances, while thin black lines represent higher resonance contributions. The horizontal bar in the upper left corner shows the range of the Gamow window for the $^{11}C(\alpha,p)^{14}N$ reaction, *i.e.*, 0.23–1.24 MeV, corresponding to T_9 =0.2–1.

which were not included in the previous studies of SN nucleosynthesis, the uncertainties of thermally averaged reaction rate could be as large as 1−2 orders of magnitude at $T_9 \sim 0.2$ as displayed in Fig. 2. The sensitivity of the nuclear abundance of ^{A}X is defined by

$$\delta(^{A}\mathrm{X}) = [Y(^{A}\mathrm{X})/Y_0(^{A}\mathrm{X}) - 1] \times 100\%, \quad (1)$$

where $Y_0(^{A}\mathrm{X})$ and $Y(^{A}\mathrm{X})$ are the abundances calculated by using the default and the enlarged or reduced rate. The results are listed in Table A1 of the Appendix. There are nine reactions with superscripts a−d in the last column, including ^{11}C$(\alpha, p)^{14}$N, whose absolute δ-values are more than 20%. Their corresponding experimental uncertainties of the reaction rate at $T = 0.2$ GK are in the last column. Although we artificially changed each reaction rate by a factor of 100 or 0.01, the error bars of measured reaction cross sections are smaller, except for our target reaction ^{11}C$(\alpha, p)^{14}$N (No. 35 in Table A1), ^{11}C$(n, p)^{11}$B (No. 32), and ^{11}C$(n, 2\alpha)^{4}$He (No. 41) whose rates are poorly known or unmeasured at relevant low energies. Among all the 43 reactions, the ^{11}C$(\alpha, p)^{14}$N plays a predominant role in depleting ^{11}C and critically impacts on the final ^{11}B abundance.

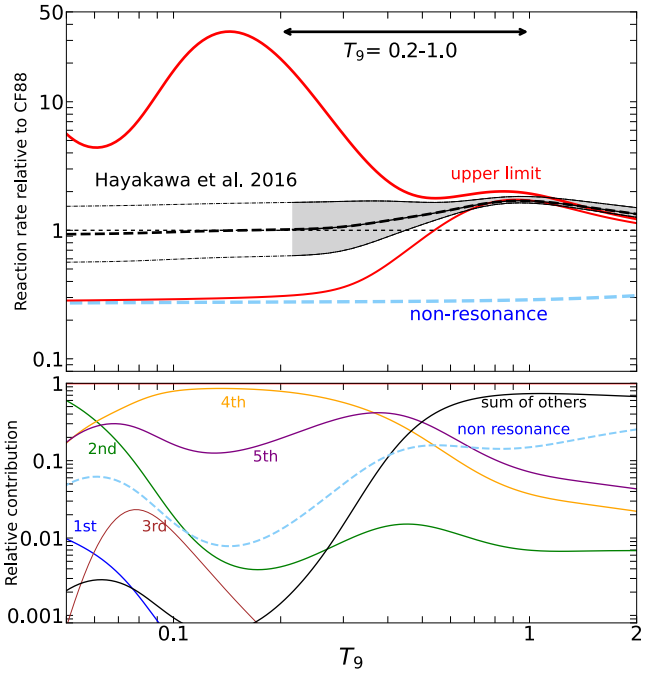

Fig. 2. (color online) The upper panel shows the ratios of the ^{11}C$(\alpha, p)^{14}$N reaction rates to the rate of CF88 as a function of temperature $T_9 = T/10^9$K. Thick red lines represent the upper and lower limits. The black hatched range represents the uncertainty in Hayakawa data. The area between the gray dashed lines shows an extrapolated band to lower temperature based on their data. The thick dashed blue line corresponds to the non-resonant contribution. The lower panel shows the contribution from the 1st-5th resonances to the total reaction rate, the sum of other resonances at higher energies, and the non-resonance contribution.

Current ^{11}C$(\alpha, p)^{14}$N rates reported in the JINA reaclib and Caughlan and Fowler [21] (we hereafter refer to CF88) are based on the experiments using indirect methods through time-reversal reaction of ^{14}N$(p, \alpha)^{11}$C [22]. The first direct measurement of ^{11}C$(\alpha, p)^{14}$N reaction rates has been performed by Hayakawa *et al.* [23]. These two experiments provide the data on this reaction, in Fig. 1, which shows the S-factor vs. the center-of-mass energy $E_{\mathrm{c.m.}}$ (hereafter abbreviated as E) beyond 0.6 MeV. Blue crosses are from direct measurement [23] (hereafter referred to as the Hayakawa data), and black dots are from inverse reaction experiment [22] (hereafter referred to as the Ingalls data). We note here that according to the energy levels of the compound state of ^{15}O [24], there are still five resonances below E = 0.5 MeV. The featured temperature for ^{11}C and ^{11}B production in the SN explosion environment is $T_9 = (T/10^9\mathrm{K}) = 0.2$−1 [5]. The corresponding Gamow peak energy (*i.e.*, the energy range where nuclear reactions operate most effectively, see Ref. [25].) is $E_0 = (bkT/2)^{2/3} = 0.23$ MeV with $b^2 = E_G = 2\mu(\pi e^2 Z_{^{11}\mathrm{C}} Z_\alpha/\hbar)^2$ at $T_9 = 0.2$, which is much lower than 0.5 MeV. Therefore, five low-energy resonances below 0.5 MeV make an additional contribution to the reaction S-factor of ^{11}C$(\alpha, p)^{14}$N, and the uncertainty of this reaction rate at low temperature needs to be verified.

A. Astrophysical *S*-factor and thermonuclear reaction rate

The total cross-section consists of both non-resonant and resonant parts:

$$\begin{aligned}\sigma_{\mathrm{tot}}(E) &= \sigma_{\text{non-res}}(E) + \sigma_{\mathrm{res}}(E), \\ &= \frac{\exp(-2\pi\eta)}{E}\{S_{\text{non-res}}(E) + S_{\mathrm{res}}(E)\}, \end{aligned} \quad (2)$$

where $S(E)$ is so-called astrophysical S-factor, η is the Sommerfeld factor, $\eta = Z_{^{11}\mathrm{C}} Z_\alpha e^2/\hbar v$, $\lambda\!\!\!^{-2} = \lambda/2\pi = \hbar/\sqrt{2\mu E}$ is the de Broglie wavelength, and μ is the reduced mass of ^{11}C and α particle. We take a simple form of non-resonant S-factor

$$S_{\text{non-res}}(E) = \exp(A \times E + B), \quad (3)$$

following CF88 [21], where A and B are treated as free parameters and calibrated to best fit the experimental data at higher energies $E \geq 2.5$ MeV (Fig. 1). The resonant S-factor is given by

$$S_{\rm res}(E) = \exp(+2\pi\eta)\times {\rm E}\times \sum_{\rm i} \pi\lambda^2\omega_{\rm i}\frac{\Gamma^{\rm i}_{\alpha}(E)\Gamma^{\rm i}_{p}(E)}{(E-E_{\rm i})^2+{\Gamma^{\rm i}_{\rm tot}}^2(E)/4}, \tag{4}$$

in the Breit-Wigner formula [25] with the information of resonances of ^{15}O [24], where $\omega_{\rm i} = (2J_{\rm i}+1)/\{[2J(^{11}{\rm C})+1][2J(^{4}{\rm He})+1]\}$ is the statistical weight factor, i is the label of the corresponding resonance and $E_{\rm i}$ is the corresponding resonance energy, $J_{\rm i}(^{15}{\rm O})$ is the spin of the corresponding compound state of ^{15}O, and $J(^{11}{\rm C}) = 3/2$ and $J(^{4}{\rm He}) = 0$ are the spins of the corresponding ground states of ^{11}C and ^{4}He, respectively. $\Gamma^{i}_{\alpha}(E) = 2\gamma^2_{\alpha}P_{\alpha}(E;l)\theta^2_{\alpha}$ is the partial width for the α-entrance channel, and γ^2_{α} is the reduced width. In this article, we take $\gamma^2_{\alpha} = 3\hbar^2/2\mu R^2$ and R is set to be the channel radius [26]. $P_{\alpha}(E;l)$ is the Coulomb penetration factor of the α particle in the $^{11}{\rm C}+\alpha$ system, which depends on the energy above the threshold and the corresponding orbital angular momentum l for each resonance. The l value depends on the difference between $J(^{11}{\rm C})$ and $J_{\rm i}(^{15}{\rm O})$, and it is constrained by parity conservation for each resonance. The Coulomb penetration factor is calculated by solving the Schrödinger equation. In this study, we applied the Coulomb function to calculate the penetration factor (Chap.9 of [27])

$$P_{\alpha}(E,l) = \frac{kR_{\rm i}}{(F^2_l+G^2_l)}, \tag{5}$$

where F_l and G_l are the regular and irregular Coulomb functions [1]. The channel radii of entrance and exit channels are 3.92 fm for ^{11}C+α and 3.35 fm for ^{14}N+p, respectively [28, 29]. The dimensionless reduced width θ^2_{α} is taken to be a parameter ranging from 0 to 1 for the lowest five resonances (see Table 1).

$\Gamma^{\rm i}_{p}(E_{\rm i}) = \Gamma^{\rm i}_{\rm tot}(E_{\rm i}) - \Gamma^{\rm i}_{\alpha}(E_{\rm i})$ is the partial width for the proton-emission channel at the corresponding resonance energy, and $\Gamma^{\rm i}_{p}(E) = \Gamma^{\rm i}_{p}(E_{\rm i})P_p(E;l)/P_p(E_{\rm i};l)$ is applied to the energies out of resonance energy. $\Gamma^{\rm i}_{\rm tot}$ is the total width which is given by the measured ^{15}O resonance width [24]. E_x is the excitation energy of the corresponding resonance $E_x = E_{\rm i} + S_{\alpha}$ with the α threshold energy $S_{\alpha} = 10.219$ MeV [30] in the entrance α-channel. For the S-factor at $E > 0.6$ MeV, since $E_{\rm i}$ and $\Gamma_{\rm tot}$ are known [24] as summarized in Table 1 and $\sigma_{\rm tot}(E)$ is given experimentally [22, 23], the only free parameters are θ^2_{α} in addition to A and B of the non-resonant S-factor.

B. New ^{11}C$(\alpha,p)^{14}$N reaction rate

To match the experimental data of S-factor in the Breit-Wigner form, we applied the χ^2-fitting method in our study to determine the values of θ^2_{α} at energy $E > 0.6$ MeV for the resonances $i = 6-18$ in Table 1, as well as parameters A and B associated with non-resonant contribution. The fitting results for θ^2_{α} values are summarized in Table 1, and $A = -0.640$ MeV^{-1} and $B = 0.484$. We applied the Wigner limit $\theta^2_{\alpha} = 1$ for the lowest five resonances to estimate the conservative upper limit of ^{11}C$(\alpha,p)^{14}$N S-factor. $\theta^2_{\alpha} = 0$ was assumed for the lower limit of resonant contribution from $i = 1-5$.

Table 1. Resonance **parameters** of the excited status of ^{15}O above the $^{11}{\rm C}+\alpha$ threshold energy. The excitation energy E_x of compound state ^{15}O, resonance energy E_i, spin and parity J^{π}, and total widths $\Gamma^{\rm i}_{\rm tot}$ from Ajzenberg-Selove (1991) [24]. The dimensionless reduced width θ^2_{α} for the other resonances at higher excitation energies are the results from χ^2-fitting to the measured cross sections at $E_{\rm c.m.} \geq 0.6$ MeV as shown in Fig. 1. Note that in our upper and lower limits of reaction rate, the θ^2_{α} values for the 1$^{\rm st}$-5$^{\rm th}$ resonances are 1 and 0, respectively. $E_x = E_{\rm i} + S_{\alpha}$ with the threshold energy $S_{\alpha} = 10.219$ MeV in the entrance α-channel.

No.	E_x/MeV	$E_{\rm i}$/MeV	J^{π}	$\Gamma^{\rm i}_{\rm tot}$/keV	θ^2_{α}
1	10.290	0.071	5/2$^-$	3	–
2	10.300	0.081	5/2$^+$	11	–
3	10.416	0.197	9/2$^+$	2	–
4	10.480	0.261	3/2$^-$	25	–
5	10.506	0.287	3/2$^+$	140	–
6	10.917	0.698	7/2$^+$	90	0.00E+00
7	10.938	0.719	1/2$^+$	99	3.88E-01
8	11.025	0.806	1/2$^-$	25	0.00E+00
9	11.151	0.932	1/2$^+$	10	7.03E-01
10	11.218	0.999	3/2$^+$	40	8.71E-03
11	11.569	1.350	5/2$^-$	20	1.38E-01
12	11.616	1.397	3/2$^-$	80	1.39E-02
13	11.748	1.529	5/2$^+$	99	7.35E-02
14	11.846	1.627	5/2$^-$	65	1.24E-01
15	11.980	1.761	5/2$^-$	20	0.00E+00
16	12.129	1.910	5/2$^+$	200	1.00E-01
17	12.255	2.036	5/2$^+$	135	1.12E-02
18	12.471	2.252	5/2$^-$	77	0.00E+00

In Fig. 1 we present the fitted ^{11}C$(\alpha,p)^{14}$N S-factor, together with experimental data from Ingalls data (black dots) and Hayakawa data (blue cross). The thick red and thin green lines are the upper and lower limits, respectively. The dashed blue line is the non-resonant contribution. Thin red curves are the contributions from the lowest five resonances, while thin black curves represent those from the higher resonances. The horizontal bar in the upper left corner shows the range of the Gamow win-

1) calculation method is from website: http://www.fresco.org.uk/programs/barnett/index.htm

dow for the $^{11}C(\alpha,p)^{14}N$ reaction, *i.e.*, 0.23–1.24 MeV, corresponding to T_9 =0.2–1.

Our theoretical *S*-factors at $E\sim 0.6$ MeV (5^{th} and 6^{th}), 1.1−1.3 MeV (between resonances the 10^{th} and 11^{th}) and ~1.6 MeV (13^{th} and 14^{th}) underproduce Ingalls data because these energies are out of known resonance-energies and because the observed total widths of nearby resonances are narrow (see Table 1). For the same reasons, the theoretical *S*-factor underproduces Hayakawa data around $E\sim 1.2$−1.3 (between 10^{th} and 11^{th} resonances) MeV. Our *S*-factor near the resonance at $E\sim 1.910$ MeV (16^{th}) cannot fit the resonance shape of Ingalls data because total width is too large $\Gamma_{tot}^{i=16}$ = 200 keV. We adopt the non-resonant *S*-factor in the same parametrization as Caughlan and Fowler (1988), which fits the average behavior of *S*-factors rather well at higher energies 2.5 MeV $< E$. As a consequence of the χ^2-fitting in terms of extrapolated smooth non-resonant *S*-factor to the low energies plus resonance contributions, our total *S*-factor overproduces the data at $E\sim 0.8$−0.9 MeV. Although there is a resonance at E = 0.806 MeV with $J^\pi = 1/2^-$, the incident *s*-wave between $^{11}C(3/2^-)$ and $^4He(0^+)$ cannot form this resonance and the *d*-wave is the smallest orbital angular momentum to form this resonance. However, at this low energy E < 1.0 MeV, *d*-wave could not contribute effectively. Therefore, the dimensionless reduced width of this resonance turns out to be almost zero in our χ^2 fit (8^{th} of Table 1).

With this *S*-factor, we calculated the thermonuclear reaction rate:

$$N_A\langle\sigma v\rangle_{tot} = N_A\left(\frac{8}{\pi\mu}\right)^{1/2}\frac{1}{(kT)^{3/2}}\int_0^\infty \exp(-2\pi\eta) \times S_{tot}(E)\exp(-E/kT)\mathrm{d}E, \quad (6)$$

The upper panel of of Fig. 2 shows the ratio of our new estimated $^{11}C(\alpha,p)^{14}N$ reaction rate to the rate of CF88. Red lines represent the upper and lower limits. The black solid line and hatched region represent the ratio of the rate to CF88 and its uncertainty from Hayakawa data. The calculated upper and lower rates of $^{11}C(\alpha,p)^{14}N$ are given in Table A2, together with the central value from Hayakawa data. Our result agrees with this estimation at around $T_9 = 0.7-2$, although slightly higher than the CF88 rate. Because of the newly added five resonances at lower energies, our estimated rate significantly differs from the CF88 rate at $T_9 \le 0.6$. In our SN model, the featured temperature for ^{11}C production is about $T_9 = 0.2-1$, where the estimated uncertainty can be different from others as much as one order of magnitude. This uncertainty calls for a more precise measurement of this reaction rate in the astrophysically interesting temperature range. In the lower panel of Fig. 2, we show each contribution from the 1st-5th resonances to the total reaction rate, the sum of the other resonances (black line) at higher energies, and the non-resonant contribution (blue dashed line). It is shown that the 4^{th} and 5^{th} resonances in Table 1 and Fig. 1 dominate the total reaction rate at $T_9 = 0.2-0.5$.

Hayakawa data takes account of resonances at $E = 2.5-4.5$ MeV in the estimated reaction rate as shown in Fig. 1, while we do not consider these resonances because the relevant Gamow window energy for the $^{11}C(\alpha,p)^{14}N$ reaction is much lower, $E = 0.23-1.24$ MeV, as shown by the arrows in Fig. 1, corresponding to the temperature $T_9 = 0.2-1$ in Fig. 2. Therefore, there is a slight difference between our rates and theirs at $T_9 > 1.5$. We confirmed that the deviation between the two rates around $T\sim 2$ GK does not change the final ^{11}C abundance in our SN model calculation.

The purpose of the present study is to set the upper and lower limits to the reaction rate for $^{11}C(\alpha,p)^{14}N$ which affects the astrophysical uncertainty in the $^{11}B/^{10}B$ ratio to be measured in SiC X grains. Using the larger rate for this reaction, ^{11}C is more strongly destroyed. We therefore assume the incoherence among resonant and non-resonant components in the total *S*-factor by ignoring the interference in order to set a conservative upper limit, leading to the maximum effect on destruction. On the other hand, the lower limit could be smaller than the present estimate ignoring the interference. Although the thermal average of the *S*-factor or equivalently the cross section tends to smear out the interference effect on the calculated reaction rate, it is an interesting question to constrain a more reliable lower limit to the *S*-factor both experimentally and theoretically. The present study suggests and motivates the importance of further studies of this reaction in the future.

III. IMPLICATIONS IN SUPERNOVA NUCLEOSYNTHESIS

A. SN model and ν-interactions

To demonstrate the impact of the $^{11}C(\alpha,p)^{14}N$ reaction and its sensitivity to the SN explosive nucleosynthesis, we incorporate the upper and lower limits of the reaction rate into our CCSN nucleosynthesis model. This SN model is the same as that used in [15] based on pre-SN model [31] and the hydrodynamic model of [5], which is a successful model for SN 1987A with a 20 $M_\odot$ and metallicity $Z = Z_\odot/4$ progenitor star. The hydrodynamic model simulates the temperature and density evolution during the explosion (see [5] for the temperature and density profile). This calculation stops at 50 s after the core bounce. After 50 s, the temperature and density become very low, and most nuclear reactions do not proceed anymore, except for β decays. The ν-process such as ν+^{12}C and ν+^4He [5, 32] are included. We also include

the newly estimated ν+^{16}O and ν+^{20}Ne reaction rates from a new shell model study [33]. The effects of neutrino flavor change, such as MSW effect [13] and collective flavor oscillation effect [6], have also been considered in the present model. The neutrino total energy is 3×10^{53} erg, and the decay timescale of neutrino luminosity is 3 s. The initial neutrino temperatures shown in $E=kT$ for ν_e, $\bar{\nu}_e$ and ν_x are 3.2, 5.0 and 6.0 MeV, respectively [32] where x stands for the μ- and τ-neutrinos and their anti-particles. All neutrino flavors are assumed to be equally partitioned in the initial luminosities, and their spectra obey Fermi-Dirac distribution with zero-chemical potentials.

In the measured ^{12}C$(\nu_e,e^-)^{12}$N$_{g.s.}$ and ^{12}C$(\nu,\nu')^{12}$C* reaction cross sections, uncertainties in charged current (CC reaction induced by the exchange of $W^{\pm}$ bosons) and neutral current (NC reaction induced by the exchange of neutral Z^0 bosons) interaction reactions are ±10% and ±20%, respectively [34]. In this study, we also assumed that ν-induced reaction cross sections for ν+^{4}He, ν+^{12}C, ν+^{16}O and ν+^{20}Ne are subject to the same uncertainties of ± 10% and ± 20% for CC and NC, respectively.

B. Effects of reaction uncertainties on the SN nucleosynthesis of *A*=10 and *A*=11 nuclei

Figure 3 shows the calculated mass fractions of (a)^{10}B, (b)^{10}C ($\tau_{1/2}$ = 19.30 secs), (c)^{11}B and (d)^{11}C ($\tau_{1/2}$ = 20.34 mins) at 50 s after the CCSN explosion started as a function of mass coordinate M_r in the units of $M_\odot$. For the convenience of comparison with other SN models, we adopted the same definition of the layers as Meyer *et al.* (1995) [35] and Yao *et al.* (2025) [15], *i.e.*, we divide the stellar interior into five regions, O/Ne, O/C, C/He, He/C, and He/N layers, marked as I~V, which depend on the most abundant nuclei in each layer. The blue and red lines represent the results under normal (blue) and inverted (red) neutrino mass hierarchies, respectively. The solid lines represent the central values (*i.e.*, with ^{11}C$(\alpha,p)^{14}$N rate from Hayakawa data). The associated bands of the ^{11}C abundance present the calculated results including uncertainties of both ^{11}C$(\alpha,p)^{14}$N and ν-induced reactions. The larger rate of the ^{11}C$(\alpha,p)^{14}$N reaction results in more efficient destruction of ^{11}C, while the larger rate of the ν-induced reactions like ^{12}C$(\nu_i,\nu_i n)^{11}$C

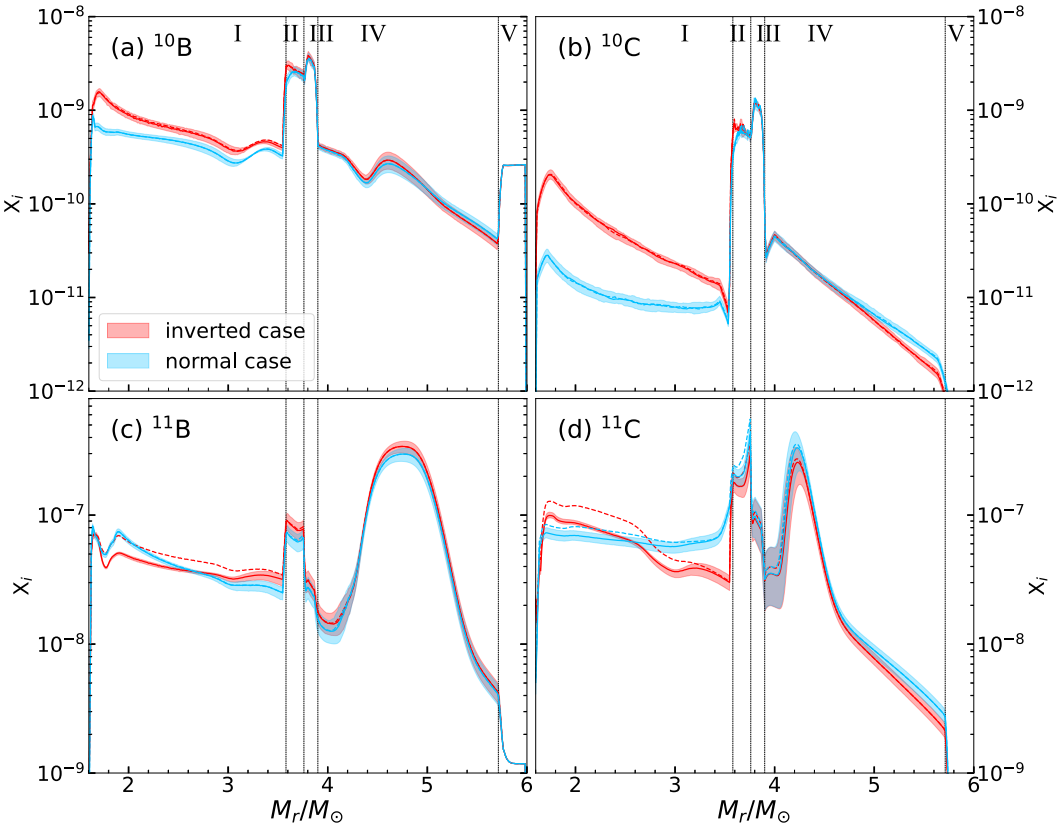

Fig. 3. (color online) The mass fraction of (a)^{10}B, (b)^{10}C, (c)^{11}B, and (d)^{11}C at 50 s after the core-bounce in the SN model calculation. The red and blue colors represent the inverted and normal hierarchies of the neutrino mass. The solid lines indicate the central values. The uncertainties of isotopic production are displayed by the colored bands, which are induced by the uncertainties of ^{11}C$(\alpha,p)^{14}$N reaction rate and the ν-induced reaction rate. The dashed lines represent the results using the CF88 rate for ^{11}C$(\alpha,p)^{14}$N. Note that the vertical axes in each panel are of different scales.

results in more efficient production of ^{11}C, and vice versa. Because of this mechanism, the lower limit of the ^{11}C abundance in Fig. 3 (d) corresponds to the upper limit of the $^{11}C(\alpha, p)^{14}N$ rate and lower limit of the ν-induced reaction rates, *i.e.* ±10% (CC) and ±20% (NC), vice versa, independently of the neutrino mass hierarchy. We also present the calculated results (dashed lines) using the $^{11}C(\alpha, p)^{14}N$ rate from CF88.

The ^{10}B and ^{10}C are mainly produced in regions II and III, as shown in Fig. 3 (a) and (b), while ^{11}B and ^{11}C are mainly produced in regions II and IV where plenty of ^{4}He exist (see Fig. 3 (c) and (d)). In our calculation, most of ^{11}B is produced via $^4He(\nu,p)^3H(\alpha,\gamma)^7Li(\alpha,\gamma)^{11}B$ and destroyed via $^{11}B(\alpha,n)^{14}N$. Similarly, ^{11}C is mostly involved in the reaction chain of $^4He(\nu,n)^3He(\alpha,\gamma)^7Be(\alpha,\gamma)^{11}C$ and subsequent destruction by $^{11}C(\alpha, p)^{14}N$. Both ^{11}B and ^{11}C mass fractions calculated by using our new rate (solid lines) are lower than those obtained by adopting CF88 rate (dashed lines) at $M_r < 4.3\ M_\odot$, particularly in O/Ne (region I) and O/C (region II) layers, for both normal and inverted hierarchies. This is because our new $^{11}C(\alpha, p)^{14}N$ rate is higher than CF88 and ^{11}C is destroyed more efficiently at temperatures $T_9 > 0.6$ when the shock arrives at these regions I and II (see Fig. 2). Although ^{10}B and ^{10}C abundances are subject primarily to the uncertainties of ν-induced reactions, ^{11}B and ^{11}C abundances depend on both uncertainties of the $^{11}C(\alpha, p)^{14}N$ reaction and the ν-induced reactions.

Figure 4 (a) $\delta(^{11}B)_\nu$ and (b) $\delta(^{11}C)_\nu$ correspond to those by taking account of the uncertainties of ν-induced reactions (CC±10%, NC±20%), and Figs. 4 (c) $\delta(^{11}B)_{(\alpha,p)}$ and (d) $\delta(^{11}C)_{(\alpha,p)}$ correspond to the calculated results by taking account of the uncertainty for the $^{11}C(\alpha, p)^{14}N$ reaction rate shown in Fig. 2. The definition of $\delta(^AX)$ is similar to Eq. (1), but for the different change of the reaction rates for $^{11}C(\alpha, p)^{14}N$ displayed in Fig. 2 and ν-induced reactions of ±10% (CC) and ±20% (NC) displayed in Fig. 4. The default $^{11}C(\alpha, p)^{14}N$ rate is taken from Hayakawa data. The sensitivities $\delta(^AX)_{(\alpha,p)}$ for the CF88 rate are also shown by dashed lines in these Figures.

In general, the ^{11}B and ^{11}C abundance uncertainties arising from ν-process are limited. As in Fig. 4 (a) and (b), the $\delta(^{11}B)_\nu$ and $\delta(^{11}C)_\nu$ are less than ±20%. As for the (α, p) reaction uncertainties, it is clear that the ^{11}B abundance is not substantially affected by this reaction, as shown in Fig. 4 (c), so that the uncertainty of ^{11}B is mainly contributed by ν-induced reaction uncertainty, except for the region $3.78\ M_\odot < M_r < 4.4 M_\odot$ where the

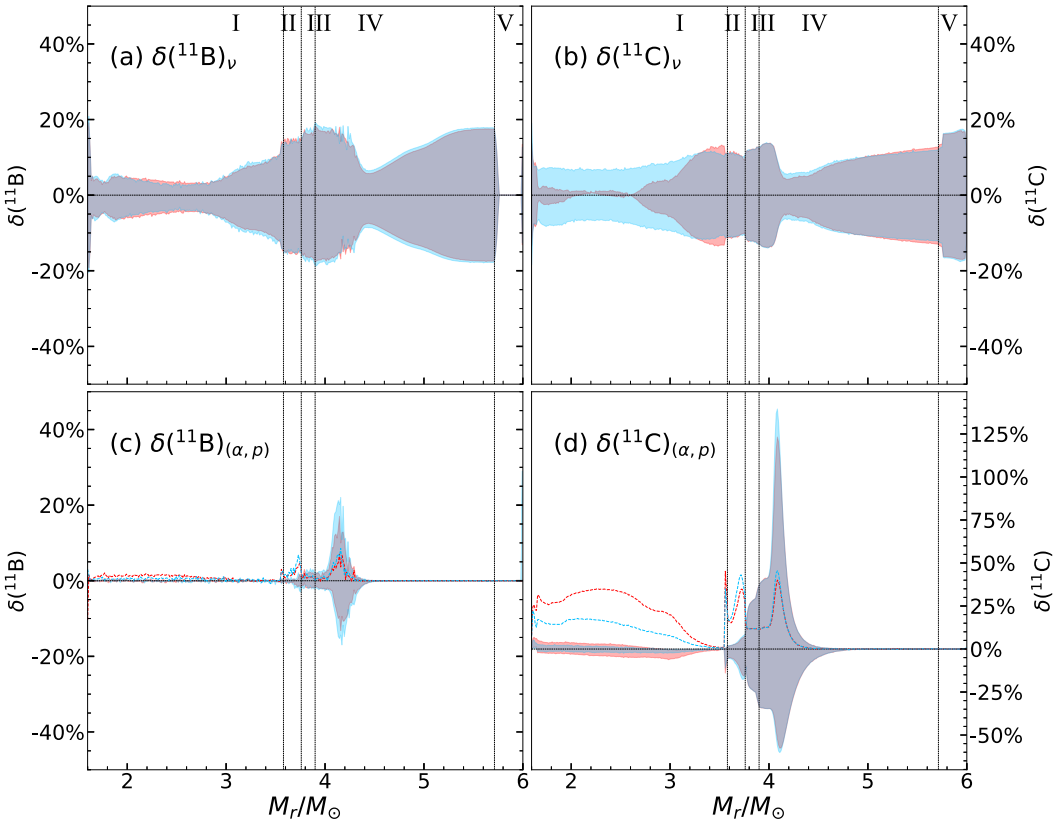

Fig. 4. (color online) The sensitivities (a) $\delta(^{11}B)_\nu$ and (b) $\delta(^{11}C)_\nu$ of the ν-induced reaction uncertainties (CC ± 10% and NC ± 20%), (c) $\delta(^{11}B)_{(\alpha,p)}$ and (d) $\delta(^{11}C)_{(\alpha,p)}$ of only the $^{11}C(\alpha, p)^{14}N$ reaction uncertainty. The line-color convention follows Fig. 3. The blue and red colors represent the results for normal and inverted hierarchies, respectively.

$\delta(^{11}\mathrm{B})_{(\alpha,p)}$ is slightly larger than $\delta(^{11}\mathrm{B})_{\nu}$.

The sensitivity of the ^{11}C abundance to (α,p) rate is as large as –50% to 140%, as shown in Fig. 4 (d), particularly in region III and inner part of region IV at 3.8 $M_\odot < M_r < 4.2\ M_\odot$. This is much larger than the sensitivity ±20% induced by the ν-process as shown in Fig. 4 (b). It is to be noted that the vertical scale of Fig. 4 (d) $\delta(^{11}\mathrm{C})_{(\alpha,p)}$ is different from the other Figs. 4 (a), (b) and (c). These results are attributed to the following mechanism of the different efficiency of destruction of ^{11}C by the $^{11}\mathrm{C}(\alpha,p)^{14}\mathrm{N}$ reaction which depends on the effective temperature in each region at the shock arrival.

In O/Ne (region I) and O/C (region II) layers, the peak temperature at the shock arrival is around $T_9 = 0.6$ (see Fig. 2 in [5]). The uncertainty of the $^{11}\mathrm{C}(\alpha,p)^{14}\mathrm{N}$ rate is tiny in these layers at this temperature as shown in Fig. 2. However, in C/He (region III) and inner part of He/C ($M_r < 4.4 M_\odot$) layers, the peak temperature is about $T_9 = 0.2 - 0.5$. The $^{11}\mathrm{C}(\alpha,p)^{14}\mathrm{N}$ rate uncertainty becomes as large as factor ~ 2 to 10 (see Fig. 2). Due to the abundant ^{4}He in these layers, $^{11}\mathrm{C}(\alpha,p)^{14}\mathrm{N}$ destroys ^{11}C as soon as ^{11}C is produced by $^7\mathrm{Be}(\alpha,\gamma)^{11}\mathrm{C}$. In the outer region of He/C layer (region IV) and He/N layer (region V) at ($M_r > 4.4 M_\odot$), the temperature becomes low enough $\boldsymbol{T_9 \sim 0.2}$ where $^{11}\mathrm{C}(\alpha,p)^{14}\mathrm{N}$ rate shows large uncertainty (Fig. 2). However, the $^{11}\mathrm{C}(\alpha,p)^{14}\mathrm{N}$ reaction is much weaker than $^7\mathrm{Be}(\alpha,\gamma)^{11}\mathrm{C}$ because the temperature becomes lower and the Coulomb barrier of α+^{11}C is higher than that of α+^{7}Be. After the explosion shock arrives at these layers, $^{11}\mathrm{C}(\alpha,p)^{14}\mathrm{N}$ destroys only small amount of ^{11}C.

C. Impact on the X grains

The isotopic signature preserved in X grains, particularly the $^{11}\mathrm{B}/^{10}\mathrm{B}$ ratio, reflects the nucleosynthesis during the explosion [15]. This ratio can reveal details about the nucleosynthesis in the SN nucleosynthesis. We note here that the formation of X grains is believed to require a carbon-rich environment, on the condition of Carbon to Oxygen ratio C/O > 1 [36]. Figure 5 illustrates the mass fraction ratio of (^{11}B+^{11}C)/(^{10}B+^{10}C) (panel a) and C/O ratio (panel b) at 50 s after the explosion as a function of mass coordinate. Regions III and IV satisfy the condition of X grain formation C/O >1. The distinct separation of the (^{11}B+^{11}C)/(^{10}B+^{10}C) ratio between the two neutrino mass hierarchies occurs near the carbon production peak region (mass coordinate $M_r \sim 4.2 - 4.6\ M_\odot$) in the He/C layer. However, the (^{11}B+^{11}C)/(^{10}B+^{10}C) ratio displays significant uncertainty in the range $3.90 M_\odot < M_r < 4.4 M_\odot$ of regions III and IV. This uncertainty is primarily attributed to the $^{11}\mathrm{C}(\alpha,p)^{14}\mathrm{N}$ as discussed previously. These reaction rate uncertainties would affect the interpretation of X grains in the meteorite study. To reduce the model uncertainty, a more precise measurement of the $^{11}\mathrm{C}(\alpha,p)^{14}\mathrm{N}$ reaction cross-section at lower energies $E_{\mathrm{c.m.}} \leq 0.6$ MeV

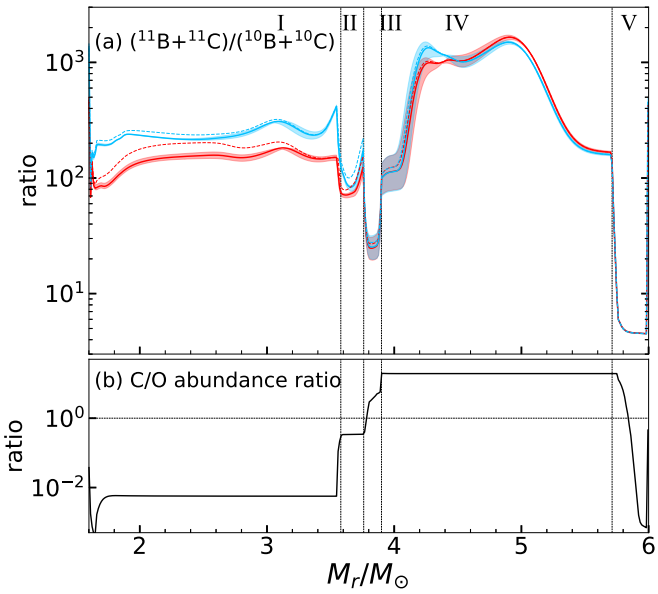

Fig. 5. (color online) The mass ratio of (a) (^{11}B+^{11}C)/(^{10}B+^{10}C) and of (b) C/O as a function of mass coordinate M_r in units of $M_\odot$ at 50 s after the core-bounce. The line-color convention follows Figs. 3 and 4.

(Fig. 1) corresponding to temperatures $T_9 \lessapprox 0.6$ (Fig. 2) is desirable in laboratory experiments. If observational evidence confirms that some X grains originated from this region, a more precise measurement of the $^{11}\mathrm{C}(\alpha,p)^{14}\mathrm{N}$ reaction rate could help improve the interpretation of X grains in the meteorite study and provide critical constraints on the neutrino mass hierarchy. For this purpose, we propose that the uncertainty of both upper and lower bounds of the $^{11}\mathrm{C}(\alpha,p)^{14}\mathrm{N}$ reaction rate should be more strictly reduced by at least 20% of its current value.

IV. CONCLUSION

We investigated both the nuclear reactions and ν-induced reactions, which play significant roles in the nucleosynthesis of A=11 nuclei in CCSNe. We found that $^{11}\mathrm{C}(\alpha,p)^{14}\mathrm{N}$ is the most sensitive nuclear reaction to the nucleosynthesis among 43 light-mass nuclear reactions which we studied in the present work. We adopted the Breit-Wigner formula and χ^2-fitting to nuclear resonance parameters of the $^{11}\mathrm{C}(\alpha,p)^{14}\mathrm{N}$ reaction, and estimated the uncertainty of temperature-dependent thermonuclear reaction rate at astrophysical temperature $T = 0.2 - 1$ GK. These uncertainties originate from the low-energy resonances in the ^{15}O compound nucleus, which could change the $^{11}\mathrm{C}(\alpha,p)^{14}\mathrm{N}$ reaction rate by one order of magnitude at the Wigner limit. We further applied our new $^{11}\mathrm{C}(\alpha,p)^{14}\mathrm{N}$ rate to our CCSN nucleosynthesis model and analyzed the sensitivity of ^{10,11}B and ^{10,11}C abundances to the $^{11}\mathrm{C}(\alpha,p)^{14}\mathrm{N}$ rate and ν-induced reaction rate. The upper limit of the $^{11}\mathrm{C}(\alpha,p)^{14}\mathrm{N}$ rate destroys ^{11}C efficiently

at $M_r = 3.78 - 4.4\ M_\odot$, which leads to a significant uncertainty in the (^{11}B+^{11}C)/(^{10}B+^{10}C) ratio. This isotopic ratio is featured in the X grains and provides insight into the origin of presolar grains and still unknown neutron-mass hierarchy. Therefore, we call for a new measurement of the $^{11}C(\alpha, p)^{14}N$ reaction cross section at astrophysical low energies $E_{\rm c.m.} \leq 0.6$ MeV.

APPENDIX

In the appendix, we provide extended data tables which are referred to in the main text.

Table A1. Sensitivity result in the $20\,M_\odot$ core-collapse supernova. The last column indicates the reaction rate uncertainties inferred from experiments. a: Valverde *et al*., Phy. Rev. C 97, 035503 (2018) [37]. b: NACRE II database [38]. c: Wang *et al*., Phy. Rev. C 43, 2 (1991) [39]. d: uncertainties unknown experimentally.

Index	Reaction name	$\delta(^{11}B)$		$\delta(^{11}C)$		uncertainty
		×100	×0.01	×100	×0.01	
1	$^{11}Be(\beta^-)^{11}B$	0.00%	0.00%	−0.02%	−0.00%	
2	$^{11}C(\beta^+)^{11}B$	24.74%	−0.77%	−91.20%	2.51%	±0.02%[a]
3	$^{11}N(\beta^+)^{11}C$	−0.00%	0.00%	0.00%	−0.01%	
4	$^{11}Be(\gamma,\alpha)^{7}Li$	0.00%	0.00%	−0.01%	−0.00%	
5	$^{12}Be(\gamma,n)^{11}B$	−0.00%	0.00%	0.01%	0.00%	
6	$^{11}B(\gamma,n)^{10}B$	0.00%	0.00%	−0.01%	0.00%	
7	$^{11}B(\gamma,p)^{10}Be$	−0.00%	0.00%	0.01%	−0.01%	
8	$^{11}B(\gamma,\alpha)^{7}Li$	−0.00%	0.00%	0.00%	−0.00%	
9	$^{12}B(\gamma,n)^{11}B$	0.03%	0.01%	−0.02%	0.02%	
10	$^{11}C(\gamma,p)^{10}B$	0.00%	0.00%	−0.00%	−0.00%	
11	$^{11}C(\gamma,\alpha)^{7}Be$	0.00%	0.00%	−0.00%	−0.01%	
12	$^{12}C(\gamma,n)^{11}C$	−0.00%	0.00%	0.00%	−0.00%	
13	$^{12}C(\gamma,p)^{11}B$	−0.00%	0.00%	0.00%	−0.01%	
14	$^{12}N(\gamma,p)^{11}C$	0.01%	−0.01%	1.14%	−1.59%	
15	$^{7}Li(\alpha,\gamma)^{11}B$	13.97%	−33.01%	2.99%	4.21%	±15%[b]
16	$^{7}Be(\alpha,\gamma)^{11}C$	−2.09%	0.30%	78.25%	−20.02%	+163%[b]−60%
17	$^{10}Be(p,\gamma)^{11}B$	0.00%	−0.00%	0.00%	0.01%	
18	$^{10}B(n,\gamma)^{11}B$	0.00%	0.00%	0.00%	−0.01%	
19	$^{10}B(p,\gamma)^{11}C$	−0.01%	−0.01%	0.03%	0.01%	
20	$^{11}B(n,\gamma)^{12}B$	−0.01%	0.01%	0.01%	−0.01%	
21	$^{11}B(p,\gamma)^{12}C$	−1.94%	0.02%	0.37%	−0.01%	
22	$^{11}C(n,\gamma)^{12}C$	−0.00%	0.01%	−0.08%	−0.02%	
23	$^{11}C(p,\gamma)^{12}N$	−0.01%	−0.00%	0.02%	0.01%	
24	$^{8}Li(\alpha,n)^{11}B$	0.01%	−0.01%	−0.01%	0.00%	
25	$^{9}Be(t,n)^{11}B$	0.02%	0.00%	0.00%	−0.02%	
26	$^{8}B(\alpha,p)^{11}C$	0.00%	0.00%	−0.00%	−0.00%	
27	$^{11}B(n,t)^{9}Be$	−0.00%	−0.00%	0.00%	0.01%	
28	$^{11}B(n,\alpha)^{8}Li$	0.00%	−0.00%	−0.00%	0.02%	
29	$^{11}B(p,n)^{11}C$	−0.00%	0.00%	0.01%	−0.00%	
30	$^{11}B(\alpha,n)^{14}N$	−71.95%	26.22%	−10.85%	22.10%	±21%[b]
31	$^{11}B(\alpha,p)^{14}C$	−49.47%	6.72%	22.56%	−4.79%	±10%[c]
32	$^{11}C(n,p)^{11}B$	2.53%	−0.15%	−75.24%	4.36%	—[d]
33	$^{11}C(p,\alpha)^{8}B$	−0.00%	−0.00%	0.00%	0.01%	
34	$^{11}C(\alpha,n)^{14}O$	0.00%	−0.00%	−0.01%	0.02%	
35	$^{11}C(\alpha,p)^{14}N$	−0.99%	1.27%	−87.52%	139.93%	most uncertain[d]

Continued on next page

Table A1-continued from previous page

Index	Reaction name	$\delta(^{11}\mathrm{B})$		$\delta(^{11}\mathrm{C})$		uncertainty
		×100	×0.01	×100	×0.01	
36	$^{14}\mathrm{C}(p,\alpha)^{11}\mathrm{B}$	−0.00%	0.00%	0.00%	−0.01%	
37	$^{14}\mathrm{N}(n,\alpha)^{11}\mathrm{B}$	0.00%	−0.00%	−0.00%	0.01%	
38	$^{14}\mathrm{N}(p,\alpha)^{11}\mathrm{C}$	0.00%	0.00%	0.00%	−0.01%	
39	$^{14}\mathrm{O}(n,\alpha)^{11}\mathrm{C}$	0.02%	0.01%	2.41%	−0.11%	
40	$^{11}\mathrm{B}(p,2\alpha)^{4}\mathrm{He}$	−88.21%	102.83%	16.94%	−7.44%	±12%[b]
41	$^{11}\mathrm{C}(n,2\alpha)^{4}\mathrm{He}$	−0.87%	0.07%	−76.58%	4.89%	—[d]
42	$^{4}\mathrm{He}(2\alpha,n)^{11}\mathrm{C}$	0.00%	0.00%	−0.01%	−0.01%	
43	$^{4}\mathrm{He}(2\alpha,p)^{11}\mathrm{B}$	0.00%	0.00%	−0.01%	−0.01%	

Table A2. The $^{11}\mathrm{C}(\alpha,p)^{14}\mathrm{N}$ reaction rates in this study as a function of temperature in $T_9 \equiv 10^9$ K. The central value is taken from [23]. The upper and lower limits are calculated in this study. The rates are given in units of $\mathrm{cm^3\,s^{-1}\,mol^{-1}}$.

Temperature T_9	Central value	Upper limit	Lower limit
5.0E-02	1.22E-21	7.35E-21	3.71E-22
5.5E-02	2.71E-20	8.55E-20	5.20E-21
6.0E-02	2.80E-19	8.28E-19	5.37E-20
6.5E-02	2.20E-18	6.87E-18	4.33E-19
7.0E-02	1.42E-17	4.99E-17	2.85E-18
7.5E-02	7.61E-17	3.23E-16	1.57E-17
8.0E-02	3.13E-16	1.89E-15	7.51E-17
8.5E-02	1.15E-15	9.96E-15	3.16E-16
9.0E-02	5.18E-15	4.72E-14	1.19E-15
9.5E-02	1.91E-14	2.01E-13	4.09E-15
1.0E-01	4.36E-14	7.71E-13	1.29E-14
1.1E-01	4.57E-13	8.44E-12	1.03E-13
1.2E-01	2.90E-12	6.54E-11	6.49E-13
1.3E-01	1.48E-11	3.80E-10	3.36E-12
1.4E-01	6.43E-11	1.75E-09	1.48E-11
1.5E-01	2.40E-10	6.65E-09	5.69E-11
1.6E-01	7.46E-10	2.16E-08	1.95E-10
1.7E-01	2.14E-09	6.15E-08	6.05E-10
1.8E-01	6.80E-09	1.57E-07	1.72E-09
1.9E-01	1.85E-08	3.66E-07	4.56E-09
2.0E-01	3.77E-08	7.90E-07	1.13E-08
2.1E-01	1.01E-07	1.59E-06	2.63E-08
2.2E-01	2.25E-07	3.04E-06	5.83E-08
2.3E-01	4.33E-07	5.52E-06	1.24E-07
2.4E-01	9.61E-07	9.61E-06	2.51E-07
2.5E-01	1.63E-06	1.61E-05	4.93E-07
2.6E-01	3.47E-06	2.63E-05	9.34E-07
2.7E-01	5.55E-06	4.15E-05	1.72E-06

Continued on next page

Table A2-continued from previous page

Temperature T_9	Central value	Upper limit	Lower limit
2.8E-01	1.11E-05	6.41E-05	3.09E-06
2.9E-01	1.74E-05	9.68E-05	5.41E-06
3.0E-01	3.16E-05	1.43E-04	9.28E-06
3.1E-01	5.03E-05	2.09E-04	1.56E-05
3.2E-01	7.92E-05	3.00E-04	2.58E-05
3.4E-01	1.86E-04	5.96E-04	6.70E-05
3.6E-01	4.63E-04	1.13E-03	1.64E-04
3.8E-01	1.02E-03	2.09E-03	3.82E-04
4.0E-01	1.88E-03	3.74E-03	8.46E-04
4.2E-01	4.01E-03	6.54E-03	1.79E-03
4.4E-01	7.59E-03	1.12E-02	3.63E-03
4.6E-01	1.31E-02	1.89E-02	7.08E-03
4.8E-01	2.43E-02	3.13E-02	1.33E-02
5.0E-01	3.78E-02	5.09E-02	2.41E-02
5.2E-01	6.78E-02	8.15E-02	4.24E-02
5.4E-01	1.01E-01	1.28E-01	7.22E-02
5.6E-01	1.71E-01	1.99E-01	1.20E-01
5.8E-01	2.49E-01	3.03E-01	1.93E-01
6.0E-01	3.95E-01	4.55E-01	3.04E-01
6.5E-01	1.03E+00	1.17E+00	8.58E-01
7.0E-01	2.41E+00	2.76E+00	2.14E+00
7.5E-01	5.14E+00	5.94E+00	4.82E+00
8.0E-01	9.92E+00	1.19E+01	9.92E+00
9.0E-01	3.53E+01	3.92E+01	3.39E+01
1.0E+00	9.34E+01	1.05E+02	9.31E+01
1.1E+00	2.27E+02	2.43E+02	2.17E+02
1.2E+00	4.86E+02	4.98E+02	4.50E+02
1.3E+00	9.43E+02	9.37E+02	8.50E+02
1.4E+00	1.70E+03	1.64E+03	1.50E+03
1.5E+00	2.86E+03	2.73E+03	2.50E+03
1.6E+00	4.54E+03	4.33E+03	3.98E+03
1.7E+00	7.12E+03	6.61E+03	6.09E+03
1.8E+00	1.08E+04	9.76E+03	9.01E+03
1.9E+00	1.55E+04	1.40E+04	1.29E+04
2.0E+00	2.15E+04	1.95E+04	1.81E+04
2.1E+00	2.99E+04	2.66E+04	2.48E+04
2.2E+00	3.98E+04	3.56E+04	3.31E+04
2.3E+00	5.24E+04	4.66E+04	4.34E+04
2.4E+00	6.78E+04	5.99E+04	5.59E+04
2.5E+00	8.56E+04	7.58E+04	7.09E+04

References

[1] M. Meneguzzi, J. Audouze, and H. Reeves, Astronomy & Astrophysics **15**, 337 (1971)
[2] H. Reeves, Rev. Mod. Phys. **66**, 193 (1994)
[3] A. Heger, E. Kolbe, W. C. Haxton *et al*., Phys. Lett. B **606**, 258 (2005)
[4] S. E. Woosley and T. A. Weaver, ApJS **101**, 181 (1995)
[5] M. Kusakabe, M. K. Cheoun, K. S. Kim *et al*., Astrophys. J. **872**, 164 (2019)
[6] H. Ko, D. Jang, M. K. Cheoun *et al*., Astrophys. J. **937**, 116 (2022)
[7] S. Amari, P. Hoppe, E. Zinner, Lewis *et al*., Astrophys. J. **394**, L43 (1992)
[8] L. R. Nittler, S. Amari, E. Zinner *et al*., Astrophys. J. **462**, L31 (1996)
[9] N. Liu, J. Barosch, L. R. Nittler *et al*., Astrophys. J. Lett. **920**, L26 (2021)
[10] P. Hoppe, K. Lodders, R. Strebel *et al*., Astrophys. J. **551**, 478 (2001)
[11] W. Fujiya, P. Hoppe, and U. Ott, Astrophys. J. Lett. **730**, L7 (2011)
[12] K. Lodders, H. Palme, and H. P. Gail, Landolt Börnstein **4B**, 712 (2009)
[13] T. Yoshida, T. Kajino, H. Yokomakura *et al*., Astrophys. J. **649**, 319 (2006)
[14] N. Prantzos, Astronomy & Astrophysics **542**, A67 (2012)
[15] X. Yao, T. Kajino, Y. Luo *et al*., Astrophys. J. **980**, 247 (2025)
[16] E. M. Burbidge, G. R. Burbidge, W. A. Fowler *et al*., Rev. Mod. Phys. **29**, 547 (1957)
[17] B. Pagel, *Nucleosynthesis and Chemical Evolution of Galaxies*, 2nd ed. (Cambridge University Press, 2009)
[18] N. Liu, L. R. Nittler, C. M. O. Alexander *et al*., Science Advances **4**, eaao1054 (2018)
[19] N. Liu, M. Lugaro, J. Leitner *et al*., Space Sci. Rev. **220**, 88 (2024)
[20] R. H. Cyburt, A. M. Amthor, R. Ferguson *et al*., ApJS **189**, 240 (2010)
[21] G. R. Caughlan and W. A. Fowler, At. Data Nucl. Data Tables **40**, 283 (1988)
[22] P. D. Ingalls, J. S. Schweitzer, B. D. Anderson *et al*., Phys. Rev. C 524 (1976)
[23] S. Hayakawa, S. Kubono, D. Kahl, *et al*., Phys. Rev. C **93**, 065802 (2016)
[24] F. Ajzenberg-Selove, Nucl. Phys. A **523**, 1 (1991)
[25] C. A. Bertulani, *Nuclear physics in a nutshell* (Princeton University Press, Princeton, N.J, 2007)
[26] C. Iliadis, *Nuclear physics of stars*, (Wiley-VCH, Weinheim, 2007)
[27] K. Bartschat, *Computational atomic physics : electron and positron collisions with atoms and ions* (Springer, Berlin, 1996)
[28] I. Angeli and K. Marinova, At. Data Nucl. Data Tables **99**, 69 (2013)
[29] J. Zhao, B.-H. Sun, I. Tanihata *et al*., Phys. Lett. B **858**, 139082 (2024)
[30] M. Wang, W. Huang, F. Kondev *et al*., Chin. Phys. C **45**, 030003 (2021)
[31] Y. Kikuchi, M.-a. Hashimoto, M. Ono *et al*., Prog. Theor. Exp. Phys. **2015**, 063E01 (2015)
[32] T. Yoshida, T. Suzuki, S. Chiba *et al*., Astrophys. J. **686**, 448 (2008)
[33] T. Suzuki, S. Chiba, T. Yoshida *et al*., Phys. Rev. C **98**, 034613 (2018)
[34] B. E. Bodmann *et al*., Phys. Lett. B **332**, 251 (1994)
[35] B. S. Meyer, T. A. Weaver, and S. E. Woosley, Meteoritics **30**, 325 (1995)
[36] K. Lodders and B. Fegley, J r., Meteoritics **30**, 661 (1995)
[37] A. A. Valverde, M. Brodeur, T. Ahn *et al*., Phys. Rev. C **97**, 035503 (2018)
[38] Y. Xu, K. Takahashi, S. Goriely *et al*., Nucl. Phys. A **918**, 61 (2013)
[39] T. R. Wang, R. B. Vogelaar, and R. W. Kavanagh, Phys. Rev. C **43**, 883 (1991)